







Use of Evolutionary Optimization Algorithms for the Design and Analysis of Low Bias, Low Phase Noise Photodetectors

Ishraq Md Anjum , Graduate Student Member, IEEE, Ergun Simsek , Senior Member, IEEE, Seyed Ehsan Jamali Mahabadi , Member, IEEE, Thomas F. Carruthers , Member, IEEE, Curtis R. Menyuk , Life Fellow, IEEE, Joe C. Campbell , Life Fellow, IEEE, David A. Tulchinsky, Member, IEEE, and Keith J. Williams

Abstract—With the rapid advance of machine learning techniques and the increased availability of high-speed computing resources, it has become possible to exploit machine-learning technologies to aid in the design of photonic devices. In this work we use evolutionary optimization algorithms, machine learning techniques, and the drift-diffusion equations to optimize a modified uni-traveling-carrier (MUTC) photodetector for low phase noise at a relatively low bias of 5 V. We compare the particle swarm optimization (PSO), genetic, and surrogate optimization algorithms. We find that PSO yields the solution with the lowest phase noise, with an improvement over a current design of 4.4 dBc/Hz. We then analyze the machine-optimized design to understand the physics behind the phase noise reduction and show that the optimized design removes electrical bottlenecks in the current design.

Index Terms—Frequency combs, optimization, photodetectors.

I. INTRODUCTION

LOW-BIAS photodetectors are important for chip-scale frequency comb applications [1] because a low bias reduces power consumption, improves thermal performance, and simplifies the electronic design. Modern epitaxial technologies enable high-precision control of the doping and composition of compound semiconductor devices [2]. At the same time, advances in computational power and numerical techniques make it possible to design, optimize, and understand the operational mechanisms

Manuscript received 6 October 2023; accepted 31 October 2023. Date of publication 3 November 2023; date of current version 2 December 2023. This work was supported by the Naval Research Laboratory. The Work at UMBC was supported by the Naval Research Laboratory under Grant N00173-21-1-G901. (Corresponding author: *Ishraq Md Anjum*.)

Ishraq Md Anjum, Ergun Simsek, Seyed Ehsan Jamali Mahabadi, Thomas F. Carruthers, and Curtis R. Menyuk are with the Department of Computer Science and Electrical Engineering, University of Maryland Baltimore County, Baltimore, MD 21250 USA (e-mail: ianjum1@umbc.edu; simsek@umbc.edu; sjamali1@umbc.edu; tcarruth@umbc.edu; menyuk@umbc.edu).

Joe C. Campbell is with the Department of Electrical and Computer Engineering, University of Virginia, Charlottesville, VA 22904 USA (e-mail: jcc7s@virginia.edu).

David A. Tulchinsky and Keith J. Williams are with the Naval Research Laboratory, Washington, DC 20375 USA (e-mail: david.tulchinsky@nrl.navy.mil; keith.williams@nrl.navy.mil).

Color versions of one or more figures in this article are available at <https://doi.org/10.1109/JLT.2023.3330099>.

Digital Object Identifier 10.1109/JLT.2023.3330099

of these devices. Among the numerical techniques that are used to simulate photodetectors, simulations based on the drift-diffusion equations (DDEs) are a useful compromise between computationally-intensive Monte Carlo simulations and purely empirical models that are not physics-based [3], [4].

To compute the white phase noise floor and cut-off frequency in a photodetector, one approach is to calculate the impulse response of the individual electrons that are created in response to the Poisson-distributed incoming light [5], [6], but this approach is computationally time-consuming [7]. Jamali Mahabadi et al. [8] showed that it is possible to calculate phase noise by first calculating the impulse response of a photodetector from the drift-diffusion equations and take advantage of the Poisson distribution of electrons in any time slot to calculate the phase noise using simple integrals over the impulse response. Using this approach greatly reduces the computation time and simplifies both the calculation and the physical interpretation of the results. As a result, we are able to use evolutionary methods to optimize the device for low phase noise at a relatively low bias of 5 V while varying all the device layer thicknesses and doping densities.

A uni-traveling-carrier photodiode (UTC) [9], [10] mainly uses electrons as active carriers in the device, rather than both electrons and holes. As electrons have higher velocities than holes, the use of electrons as the sole carriers has made it possible to increase the speed, bandwidth and saturation current of photodetectors. A modified uni-traveling-carrier (MUTC-4) photodetector has been designed by Li et al. [11] in which the space-charge effect is reduced by adding a cliff layer between the collection layer and the absorption layer, which further improved the performance. MUTC photodetectors are widely used in frequency comb applications, RF-photonics, time and frequency metrology, and photonic low-phase-noise generation [12]. However, phase noise in photodetectors can limit the system performance in these applications [5], [13]. In particular, the low noise of an optical pulse train from an optical frequency comb can be transmitted to the microwave domain only to a limited extent due to phase noise in the photodetection process [13].

In order to achieve enhanced performance, multiple layers are used in the design of MUTC photodetectors. The number of

layers increases the number of design parameters, which makes the optimization process complex. Evolutionary optimization algorithms are very efficient in finding global minima in optimization problems that have a large search space and tens of dimensions [14]. Analysis of the optimized designs can also provide physical insight into the device dynamics. By using this inverse approach to learn about complex interactions, new and less obvious physics can be discovered and used to design better devices. In this work, we extend the prior work in which we only used particle swarm optimization (PSO) and did not provide a detailed description of the physics that led to an improved device performance [15]. Here we compare three evolutionary optimization algorithms — particle swarm optimization (PSO) [16], [17], [18], genetic algorithm (GA) [19], [20], and surrogate optimization algorithm (SO) [21], [22] — to optimize the MUTC-4 photodetector that was designed by Li et al. [11]. In all three optimization algorithms, we vary the doping densities and thicknesses of the photodetector layers while keeping the bias fixed at 5 V. We find that both PSO and SO perform well. SO generates several designs with nearly the same performance when it approaches a local minimum, while PSO still explores the solution space for the possibility of finding other local minima. We investigate in detail the optimized design that is found by the PSO algorithm to gain insight into the physics behind the optimized design. We find that at the relatively low bias of 5 V that we are considering here, electric-field “bottlenecks” can be created in the intrinsic region, which can be removed by adjusting the doping densities and thicknesses of the layers in the intrinsic region. Additionally, we find that an enhanced electric field at the layer boundaries in the photon absorption region also contributes towards the reduction of phase noise.

II. COMPUTATIONAL MODEL AND PHASE NOISE CALCULATION

We use the one-dimensional (1-D) computational model developed by Hu et al. [24] and improved upon by Simsek et al. [25], [26] that is based on the drift-diffusion equations. In order to accurately simulate the nonequilibrium phenomena, we include the physical effects — impact ionization [4], carrier recombination [27] and Franz-Keldysh effect [28]— in our simulation model. We use empirical expressions to make the electron velocity functions of electric field [29], temperature [24] and doping densities [30]. We did not include quantum confinement in the simulation model since the photodetector designs do not include quantum confined structures. The photodetector structures are around 3 μm in length, and the minimum layer thickness in the original and optimized structure is 15 nm, so that the probability of quantum tunneling is negligible.

We follow the procedure described by Jamali Mahabadi et al. [8] to calculate the phase noise. We first use the drift-diffusion equations to compute the electronic impulse response $h_e(t)$ of the device for an optical pulse that is sufficiently short that $h_e(t)$ is entirely determined by the pulse energy. We then compute the phase noise using the expression [8]

$$\langle \Phi_n^2 \rangle = \frac{1}{N_{\text{tot}}} \frac{\int_0^{T_R} h_e(t) \sin^2 [2\pi n(t - t_c)/T_R] dt}{\left\{ \int_0^{T_R} h_e(t) \cos [2\pi n(t - t_c)/T_R] dt \right\}}, \quad (1)$$

where $\langle \Phi_n^2 \rangle$ is the mean square phase fluctuation at the comb-line number n , N_{tot} is total number of electrons in the photocurrent, T_R is the repetition rate, $h_e(t)$ is the impulse response of the output current in the limit of short ($\lesssim 500$ fs) input optical pulses, and t_c is the central time of the impulse response $h_e(t)$. The impulse response is defined as

$$h_e(t) = \frac{\Delta I_{\text{out}}(t)}{\int_0^{T_R} \Delta I_{\text{out}}(t) dt}, \quad (2)$$

where ΔI_{out} is the change in the output current due to the input optical pulse. The central time is defined implicitly by the relation

$$0 = \int_0^{T_R} h_e(t) \sin \left[\frac{2\pi n}{T_R} (t - t_c) \right] dt. \quad (3)$$

In the short-optical-pulse limit, the output current impulse response only depends on the total energy in the input optical pulse and not its shape [8].

III. MUTC PHOTODETECTOR STRUCTURES

We optimized the MUTC-4 photodetector that was designed by Li et al. [11]. In Fig. 1(a) we show the original MUTC-4 structure and in Fig. 1(b) we show the optimized MUTC-4 structure found by the PSO algorithm. In this work, the output current I_{out} that is the mean of $\Delta I_{\text{out}}(t)$ is 100 μA ; the external load impedance R_{load} is 50 Ω ; the diameter of the MUTC photodetectors is 50 μm ; the pulse-width is 100 fs and the repetition frequency is 50 MHz, corresponding to setting $T_R = 20$ ns.

IV. OPTIMIZATION PROCESS

We optimized the doping levels and thicknesses of the 17 layers; hence there are 34 optimization parameters. We used the PSO, GA and SO optimization algorithms and set the phase noise as the cost function.

PSO and GA are based on principles derived from nature. PSO is inspired from a flock of birds or a swarm of bees or ants looking for food [16] while GA is inspired by Darwin’s concept of survival of the fittest [19]. In PSO, a population is initialized throughout the solution space. Each of these points are candidate solutions and are called particles. These particles are also given velocities and they move across the solution space searching for the optima. Similar to a swarm of bees, each of the particles informs the others of its findings.

In GA, an initial population evolves in a manner similar to biological evolution. The parameters to be optimized are called genes. The genes together form the chromosome. In our case, the chromosome consists of the doping concentrations and thicknesses of the 17 layers. Hence there are 34 genes that make up a chromosome. The initial population evolves through three mechanisms — selection, crossover and mutation of the genes.

SO uses machine learning techniques to accelerate the optimization process [22]. SO works by creating a statistical model of the objective function, so that the model can approximate the objective function’s output given an input. Since a single evaluation of the surrogate function takes a small amount of time, this approach is particularly effective for optimization problems

| |
|---|
| InGaAs, p+, Zn, 2.0×10^{19} , 50 nm |
| InP, p+, Zn, 1.5×10^{18} , 100 nm |
| InGaAsP, Q1.1, p+, Zn, 2.0×10^{18} , 15 nm |
| InGaAsP, Q1.4, p+, Zn, 2.0×10^{18} , 15 nm |
| InGaAs, p+, Zn, 2.0×10^{18} , 100 nm |
| InGaAs, p+, Zn, 1.2×10^{18} , 150 nm |
| InGaAs, p+, Zn, 8.0×10^{17} , 200 nm |
| InGaAs, p+, Zn, 5.0×10^{17} , 250 nm |
| InGaAs, n, Si, 1.0×10^{16} , 150 nm |
| InGaAsP, Q1.4, p+, Si, 1.0×10^{16} , 15 nm |
| InGaAsP, Q1.1, p+, Si, 1.0×10^{16} , 15 nm |
| InP, n, Si, 1.4×10^{17} , 50 nm |
| InP, n, Si, 1.0×10^{16} , 900 nm |
| InP, n+, Si, 1.0×10^{18} , 100 nm |
| InP, n+, Si, 1.0×10^{19} , 900 nm |
| InGaAs, n+, Si, 1.0×10^{19} , 20 nm |
| InP, n+, Si, 1.0×10^{19} , 200 nm |
| InP, semi-insulating substrate |

(a)

| |
|--|
| InGaAs, p+, Zn, 2.0×10^{19} , 50 nm |
| InP, p+, Zn, 1.5×10^{18} , 100 nm |
| InGaAsP, Q1.1, p+, Zn, 2.0×10^{18} , 15 nm |
| InGaAsP, Q1.4, p+, Zn, 2.0×10^{18} , 15 nm |
| InGaAs, p+, Zn, 2.0×10^{18} , 100 nm |
| InGaAs, p+, Zn, 1.0×10^{18} , 30 nm |
| InGaAs, p+, Zn, 1.0×10^{18} , 125 nm |
| InGaAs, p+, Zn, 1.0×10^{17} , 230 nm |
| InGaAs, n, Si, 1.0×10^{16} , 150 nm |
| InGaAsP, Q1.4, p+, Si, 1.0×10^{16} , 15 nm |
| InGaAsP, Q1.1, p+, Si, 1.0×10^{16} , 15 nm |
| InP, n, Si, 1.0×10^{16} , 800 nm |
| InP, n+, Si, 1.0×10^{18} , 100 nm |
| InP, n+, Si, 1.0×10^{19} , 900 nm |
| InGaAs, n+, Si, 1.0×10^{19} , 20 nm |
| InP, n+, Si, 1.0×10^{19} , 200 nm |
| InP, semi-insulating substrate |

(b)

Fig. 1. Structure of the (a) original MUTC photodetector [11] and the (b) optimized MUTC photodetector. Modified layer parameters are indicated with boldface. Blue indicates the p -region, red indicates the n -region, white indicates the i -region and grey indicates the substrate. We label each level with the material, doping type, doping density, and thickness.

where the objective function is expensive. After a user-controlled number of function evaluations, the surrogate model uses the new data to refine itself and focuses the search in the regions where the probability of finding the global optimum is high.

We ran the three optimization algorithms on the UMBC high-performance computing cluster [23] in parallel for 24 hours using the design of Li et al. [11] as our starting point. PSO generated 709 designs, GA generated 225 designs, and SO generated 374 designs. Out of the 1308 designs in total for all three algorithms PSO generated the design with the least phase noise. PSO generated better results than the other two algorithms

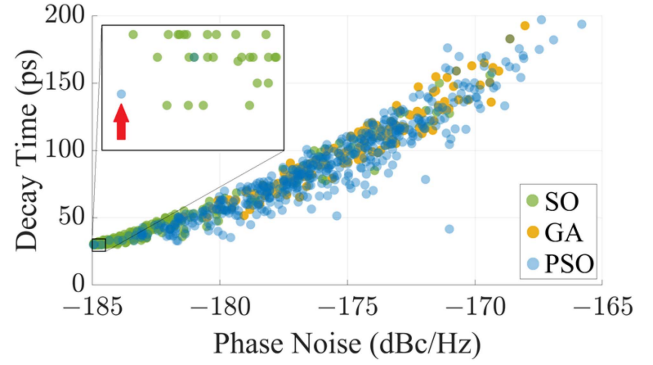


Fig. 2. Scatter plots of the designs generated by PSO, GA, and SO. The red arrow in the inset indicates the least-phase-noise design found by the PSO.

because it better explores the solution space. We rounded the parameters of the design that the PSO algorithm found to make the design suitable for fabrication, and found a further reduction in the phase noise. For PSO, we used a swarm size of 400. For GA, we set the crossover fraction that is the fraction of each population available to crossover to 0.8. For SO, we set the number of function evaluations before the surrogate model is updated to 4. For PSO and GA, we set the algorithms to stop if the relative change in the objective function is less than or equal to 1.0×10^{-6} . For SO, we set the limit of the objective function to negative infinity. Although with evolutionary optimization algorithms with such a large parameter space, finding the global optimum is not guaranteed, the improvement in the objective function becomes less than 0.3 dBc/Hz — respectively 10, 5, and 3 hours before the end of the 24 h runtime for SO, GA, and PSO. Hence it is likely that the design that PSO found is close to the optimum. We set the minimum and maximum doping densities to 1.0×10^{17} and 2.0×10^{19} respectively in the p -region, 1.0×10^{17} and 2.0×10^{19} respectively in the n -region and, 1.0×10^{16} and 2.0×10^{17} respectively in the i -region. For the layer thicknesses, we set the minimum limit to 10 nm and the maximum limit to 1000 nm.

In Fig. 2, we show scatter plots of decay time vs. phase noise. The decay time is the time that it takes the impulse response to decay to 1% of its initial value. We can see the positive correlation between phase noise and decay time of the designs [8]. In Fig. 3, we show the phase noise histograms of the designs generated by the three algorithms. If we compare the scatter plots and histograms of the three algorithms, we see that for SO, the histogram is skewed towards the low phase noise region. This skew occurred because SO reached near the low-phase-noise limit (≤ 0.3 dBc/Hz change in phase noise) in about 14 hours, which is earlier than was the case for PSO and GA. For PSO and GA, the time was about 21 and 19 hours respectively. Hence, SO was the most efficient of the three algorithms at finding designs with low phase noise, although PSO found a better design at a later time. We conclude that SO was successful in building a surrogate model of the cost function, and exploiting the active learning to concentrate searches in the regions where the probability of finding low phase noise designs is higher. In contrast to the other two algorithms, PSO explored

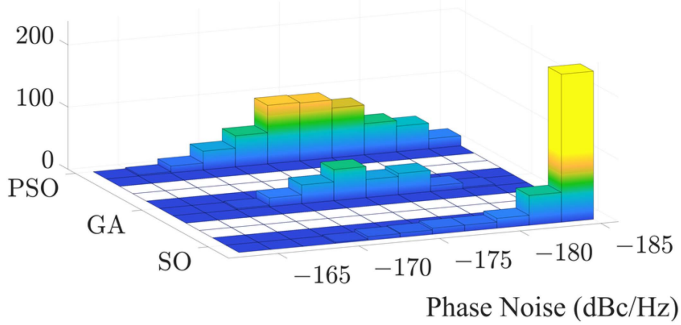
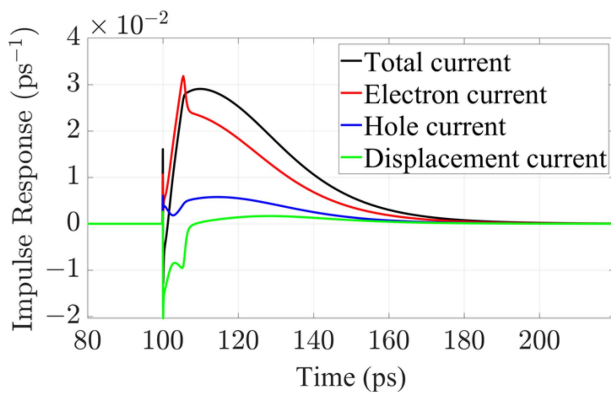
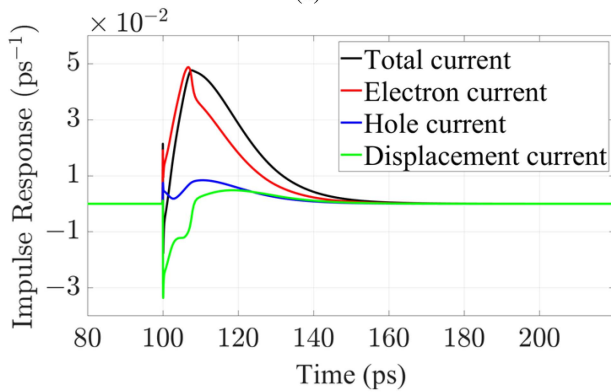


Fig. 3. Phase noise histograms of the designs generated by PSO, GA, and SO.



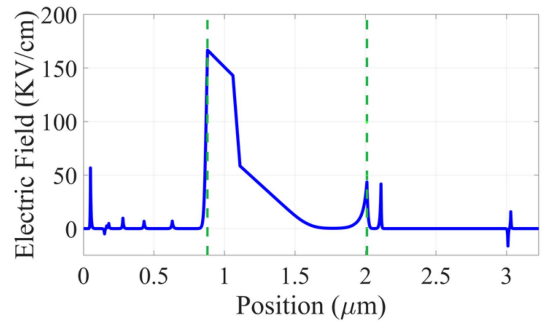
(a)



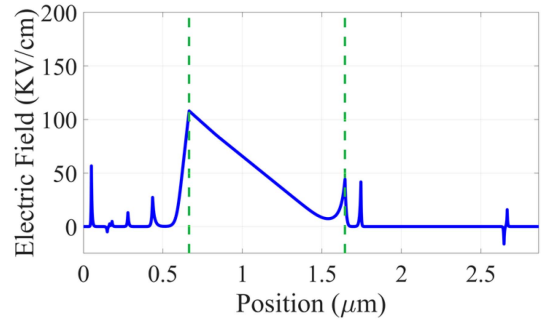
(b)

Fig. 4. Normalized impulse response (a) of the original MUTC device and (b) of the optimized MUTC device.

the solution space for a longer time and eventually found the best design. Thus, we found that SO yields a converged result more quickly than the other two algorithms by taking advantage of its machine learning acceleration. However, we also found that PSO is the most effective in finding the global optimum, but it is not as efficient as SO in reaching the low-phase-noise limit. These results suggest that if there is a constraint on computational resources and time, it is best to use SO, and if finding the global optimum has a greater priority and computing resources are not limited, it is best to use PSO.



(a)



(b)

Fig. 5. Electric field inside the (a) original MUTC device and the (b) optimized MUTC device in dark mode. Vertical green dashed lines indicate the intrinsic region.

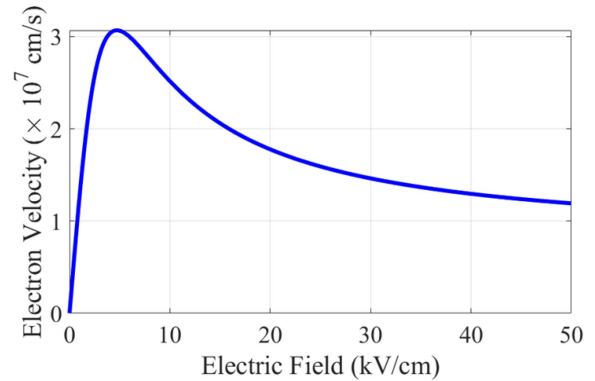


Fig. 6. Electron drift velocity variation as a function of the electric field in InGaAs.

In the design optimized using PSO, the changes are made in layers 6, 7, 8 and 12 in Fig. 1. Layer 12 in the original MUTC photodetector is merged with layer 13 in the optimized MUTC photodetector, since the doping densities of the two layers are the same. The device length of the original MUTC photodetector is 3230 nm whereas that of the new design is 2865 nm. The optimized device is about 10% thinner than the original device.

V. RESULTS AND ANALYSIS OF THE OPTIMIZED DESIGN

The electron drift velocity in the photodetector is a nonmonotonic function of the ambient electric field, as Fig. 6 indicates. Moreover, incident light injects an electron-hole

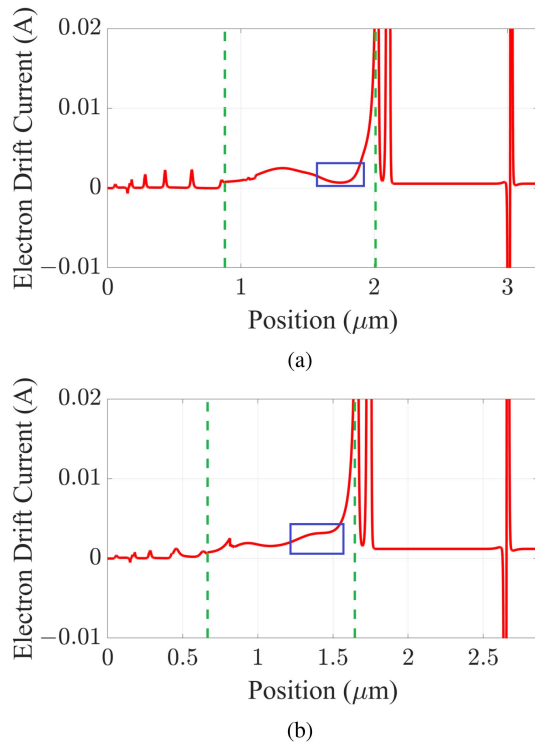


Fig. 7. Electron drift current inside (a) the original MUTC device at 105 ps and the (b) the optimized MUTC device at 107 ps showing the presence and absence of a bottleneck. Vertical dashed lines enclose the intrinsic region. The times are selected based on when the bottleneck region is reached by the photogenerated electrons.

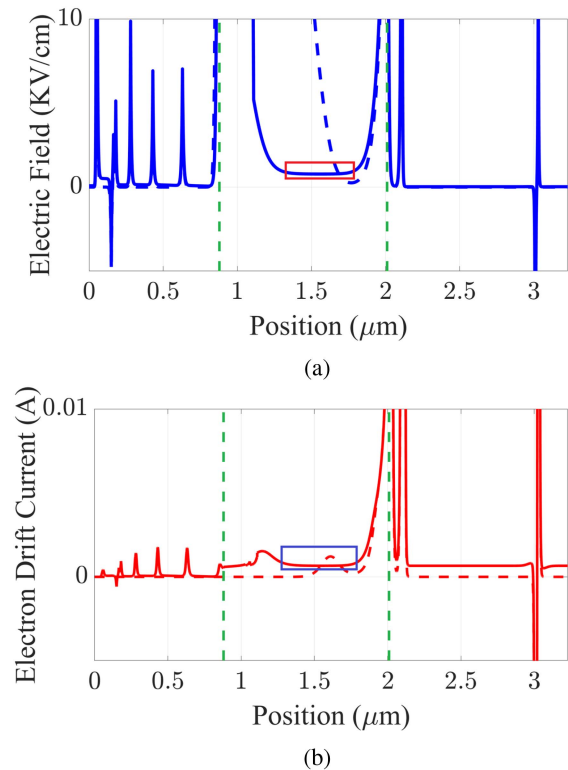


Fig. 8. (a) Electric field and (b) the electron drift current inside the original MUTC photodetector at 106 ps. The rectangles indicate the region where the electric field and electron drift current is low. The blue and red dashed lines indicate the electric field and electron drift current respectively in dark mode. Vertical green dashed lines enclose the intrinsic region.

plasma into the drift region, which also affects the electric field distribution. The transit time of electrons through the device depends on the overall field structure; a shorter transit time results in a lower phase noise. In addition, the variation in the transit time is larger, and therefore the phase noise is larger, when the slope of the electron velocity vs. field curve is larger [31]. Finding optimum thicknesses and doping levels of the layers in the intrinsic region to produce the lowest phase noise is therefore a complex process, which can be greatly aided by computer optimization and evolutionary optimization algorithms, since these algorithms are especially effective at global optimization problems involving high numbers of parameters.

We plot the impulse responses of the original and optimized design in Fig. 4(a) and (b) respectively. The original MUTC photodetector has a phase noise of -182.2 dBc/Hz, while the optimized MUTC photodetector has a phase noise of -186.6 dBc/Hz. There is an improvement of 4.4 dBc/Hz in phase noise. The original MUTC has a FWHM of 43 ps whereas the optimized MUTC has a FWHM of 27 ps. There is a reduction of 37.5% in the FWHM and a 22.3% reduction of decay time. However, there is a 10% decrease in responsivity in the optimized device. We further tested the optimized design for robustness. To address the uncertainty in epilayer growth, we randomly varied the parameters by 10% and simulated ten test cases. We consistently found an improvement in phase noise of about 4 dBc/Hz. Since the optimized design has a shorter tail, there is an improvement of 24% in the 3-dB bandwidth as well.

To test if the phase noise is affected by the optical power, we gradually increased the optical power at regular intervals and found that there is a decrease in the phase noise improvement as the optical power increases. When the optical power is doubled to 0.3 mW, the phase noise improvement decreases from 4.4 dBc/Hz to 2.2 dBc/Hz. In order to determine the photodetector's high power behavior, we calculated the saturation current of the optimized design. We found that the optimized design has a 0.4% higher saturation current than the original design.

The original MUTC design results in two low electric field regions in the intrinsic layers. One low electric field region occurs at the end of the 800 nm InP drift layer as shown in Fig. 5(a). The bottleneck created by the low-field in the electron drift current is shown in Fig. 7(a). The second low-field region is caused by the space charge effect and occurs at the middle of the drift layer at 106 ps. The low-field region and electron drift current occurring at 106 ps is shown in Fig. 8(a) and (b) respectively. The low-field region at the end of the drift region is built-in and permanent and the one at the middle occurs for a short duration while the electrons are passing through the intrinsic region. These low-electric-field regions increase the transit time and lengthen the tail of the impulse response, increasing the phase noise. In the optimized design both the low-field regions are removed, shortening the transit time and reducing the phase noise. This result is obtained by decreasing the doping density in the 50 nm InP layer and merging it with the 800 nm drift layer. We show the higher electric field and

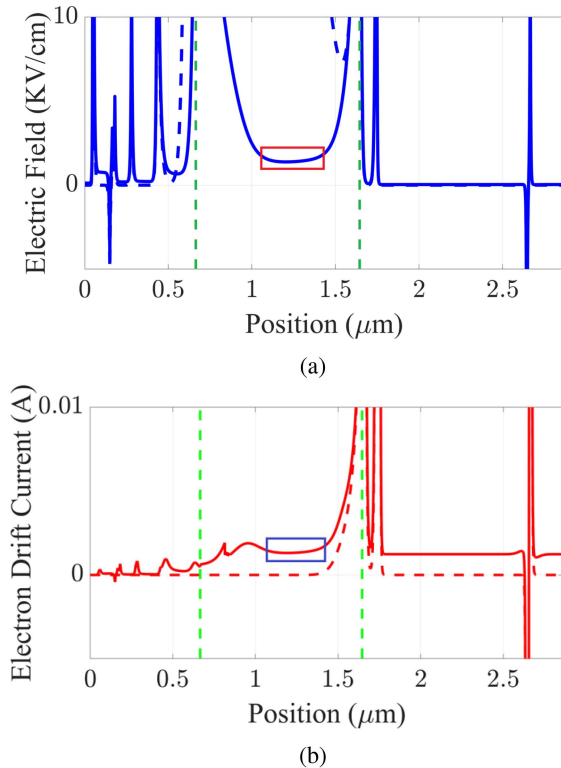


Fig. 9. (a) Electric field and (b) the electron drift current inside the optimized MUTC photodetector at 108 ps. The rectangles indicate the region where the electric field and electron drift current exceed those of the original design. The blue and red dashed lines indicate the electric field and electron drift current respectively in dark mode. Vertical green dashed lines indicate the intrinsic region.

the absence of a bottleneck in electron drift current at the end of the drift layer in the optimized design in Figs. 5(b) and 7(b) respectively. We show the higher electric field and electron drift current in the middle of the optimized design at 108 ps in Fig. 9(a) and (b) respectively. We see that in the optimized design, the electric field does not completely collapse, leading to a higher electron drift current in the intrinsic region.

The optimized electric field distribution found by PSO takes advantage of the electron velocity overshoot, removes the low-field bottlenecks, and thus minimizes the transit time and hence the phase noise. The absence of bottlenecks in the optimized electric field distribution also improves the linearity and saturation current.

The PSO algorithm suggested changes in the doping densities and thicknesses of the three layers in the photon absorption region that led to larger electric fields at the layer boundaries. This increase in the electric field and electron drift velocity assists the electrons as they move from the absorption layers in the p -region into the intrinsic region. This shortens the transit time and the tail of the impulse response, decreasing the phase noise.

If we shorten the intrinsic region length, the electron transit time decreases, but the electron RC time constant increases. The PSO algorithm found that 800 nm is the optimal length that balances this tradeoff.

VI. CONCLUSION

We have demonstrated that it is possible to optimize photodetectors using three evolutionary optimization algorithms — PSO, GA, and SO. The PSO algorithm found the device with the lowest phase noise, although it was somewhat more computationally expensive than the other algorithms. The optimized MUTC photodetector has 4.4 dBc/Hz lower phase noise than the original MUTC photodetector and is also thinner and faster. We interrogated the optimized design and gained physical insight into the dynamics of carrier transport inside the photodetector. We find that at low bias, bottlenecks are created inside the photodetector that increase the phase noise.

We thus conclude that phase noise from photodetectors can be reduced by carefully tailoring the doping levels and thicknesses of the layers, and evolutionary optimization algorithms can assist in this design process.

ACKNOWLEDGMENT

The optimization was carried out at the UMBC High Performance Computing Facility (<https://hpcf.umbc.edu>).

REFERENCES

- [1] B. Stern, S. Ji, Y. Okawachi, A. L. Gaeta, and M. Lipson, "Battery-operated integrated frequency comb generator," *Nature*, vol. 562, pp. 401–405, 2018.
- [2] M. Leszczynski, "Special issue 'advances in epitaxial materials'-editorial preface," *Materials*, vol. 11, 2020, Art. no. 2622.
- [3] K. J. Williams, R. D. Esman, and M. Dagenais, "Nonlinearities in p-i-n microwave photodetectors," *J. Lightw. Technol.*, vol. 14, no. 1, pp. 84–96, Jan. 1996.
- [4] K. J. Williams, "Microwave nonlinearities in photodiodes," PhD Dissertation, Univ. Maryland, College Park, MD, USA, 1994.
- [5] B. E. A. Saleh and M. C. Teich, *Fundamentals of Photonics*. Hoboken, NJ, USA: Wiley, 1991.
- [6] F. Quinlan, T. M. Fortier, H. Jiang, and S. A. Diddams, "Analysis of shot noise in the detection of ultrashort optical pulses," *J. Opt. Soc. Amer. B.*, vol. 30, pp. 1775–1785, 2013.
- [7] W. Sun et al., "Broadband noise limit in the photodetection of ultralow jitter optical pulses," *Phys. Rev. Lett.*, vol. 113, 2014, Art. no. 203901.
- [8] S. E. J. Mahabadi et al., "Calculation of the impulse response and phase noise of a high-current photodetector using the drift-diffusion equations," *Opt. Exp.*, vol. 27, pp. 3717–3730, 2019.
- [9] T. Ishibashi, N. Shimizu, S. Kodama, H. Ito, T. Nagatsuma, and T. Furuta, "Uni-traveling-carrier photodiodes," in *Ultrafast Electronics and Optoelectronics (13 of OSA Trends in Optics and Photonics Series)*, M. Nuss and J. Bowers, Eds. Washington, DC, USA: Optica Publishing Group, 1997, paper UC3.
- [10] T. Ishibashi and H. Ito, "Uni-traveling carrier photodiodes: Development and prospects," *IEEE J. Sel. Topics Quantum Electron.*, vol. 28, no. 2: Optical Detectors, Mar./Apr. 2022, Art. no. 3803006.
- [11] Z. Li, H. Pan, H. Chen, A. Beling, and J. C. Campbell, "High-saturation-current modified uni-traveling-carrier photodiode with cliff layer," *IEEE J. Quantum Electron.*, vol. 46, no. 5, pp. 626–632, May 2010.
- [12] T. M. Fortier et al., "Photonic microwave generation with high-power photodiodes," *Opt. Lett.*, vol. 38, pp. 1712–1714, 2013.
- [13] V. J. Urlick, Keith J. Williams, and Jason D. McKinney, *Fundamentals of Microwave Photonics*. Hoboken, NJ, USA: Wiley, 2015.
- [14] D. Simon, *Evolutionary Optimization Algorithms*. Hoboken, NJ, USA: Wiley, 2013.
- [15] I. M. Anjum, E. Simsek, S. E. J. Mahabadi, T. F. Carruthers, and C. R. Menyuk, "Design and analysis of low bias, low phase noise photodetectors for frequency comb applications using particle swarm optimization," in *Proc. IEEE Int. Topical Meeting Microw. Photon.*, 2022, pp. 1–4.
- [16] J. Kennedy and R. Eberhart, "Particle swarm optimization," in *Proc. IEEE Int. Conf. Neural Netw.*, 1995, pp. 1942–1948.

- [17] E. Mezura-Montes and C. A. C. Coello, "Constraint-handling in nature-inspired numerical optimization: Past, present and future," *Swarm Evol. Comput.*, vol. 1, no. 4, pp. 173–194, 2011.
- [18] M. E. Pedersen, *Good Parameters for Particle Swarm Optimization*. Luxembourg, Luxembourg: Hvas Laboratories, 2010.
- [19] D. E. Goldberg, *Genetic Algorithms in Search, Optimization & Machine Learning*. Boston, MA, USA: Addison-Wesley, 1989.
- [20] A. R. Conn, N. I. M. Gould, and P. L. Toint, "A globally convergent augmented Lagrangian barrier algorithm for optimization with general inequality constraints and simple bounds," *Math. Computation*, vol. 66, pp. 261–288, 1997.
- [21] L. B. Booker, D. E. Goldberg, and J. H. Holland, "Classifier systems and genetic algorithms," *Artif. Intell.*, vol. 40, pp. 235–282, 1989.
- [22] M. A. Abramson, C. Audet, J. E. Dennis Jr., and Sebastien Le Digabel, "ORTHOMADS: A deterministic MADS instance with orthogonal directions," *SIAM J. Optim.*, vol. 20, pp. 948–966, 2009.
- [23] "UMBC high performance computing facility," [Online]. Available: <https://hpcf.umbc.edu>
- [24] Y. Hu, B. S. Marks, C. R. Menyuk, V. J. Urick, and K. J. Williams, "Modeling sources of nonlinearity in a simple PIN photodetector," *J. Lightw. Technol.*, vol. 32, no. 20, pp. 3710–3720, Oct. 2014.
- [25] E. Simsek, S. E. J. Mahabadi, I. M. Anjum, and C. R. Menyuk, "A robust drift-diffusion equations solver enabling accurate simulation of photodetectors," in *Proc. Photon. Electromagn. Res. Symp.*, 2021, pp. 21–25.
- [26] E. Simsek, I. M. Anjum, and C. R. Menyuk, "Solving drift-diffusion equations on non-uniform spatial and temporal domains," *Photon. Electromagn. Res. Symp.*, 2023, pp. 3–6.
- [27] S. Selberherr, *Analysis and Simulation of Semiconductor Devices*. Berlin, Germany: Springer, 2012.
- [28] H. I. Ralph, "On the theory of Franz-Keldysh effect," *J. Phys. C: Solid State Phys.*, vol. 1, 1968, Art. no. 378.
- [29] M. Dentan and B. de Cremoux, "Numerical simulation of the nonlinear response of a p-i-n photodiode under high illumination," *J. Lightw. Technol.*, vol. 8, no. 8, pp. 1137–1144, Aug. 1990.
- [30] C. Hilsum, "Simple empirical relationship between mobility and carrier concentration," *Electron. Lett.*, vol. 10, pp. 259–260, 1974.
- [31] J. Sun, B. Xu, W. Sun, S. Zhu, and N. Zhu, "The effect of bias and frequency on amplitude to phase conversion of photodiodes," *IEEE Photon. J.*, vol. 12, Aug. 2020, Art. no. 5502010.